Formation of Hydroxyapatite Coating on Anodic Titanium Dioxide Nanotubes *via* an Efficient Dipping Treatment

LU-NING WANG and JING-LI LUO

Hydroxyapatite (HA) depositions on metallic biomedical implants have been widely applied to generate bioactive surfaces in simulated biological environments. Meanwhile, highly ordered TiO_2 nanotubes obtained *via* anodization have attracted increasing interest for biomedical applications. However, the capability to grow HA coating on TiO_2 nanotubes at room temperature remains problematic. In this study, we applied a dipping treatment for biomimetic formation of an adhesive HA coating on titanium dioxide nanotubes. The coatings formed using this procedure did not require high-temperature annealing or high supersaturation of the simulated biological condition. The as-formed TiO_2 nanotubes on titanium were treated using several dip-and-dry steps, through which the TiO_2 nanotubes were filled and covered with calcium phosphate nucleation sites. The specimens readily grew HA once immersed in the original simulated biological fluid (SBF) after little more than 12 hours. The carbonated HA coating was formed with 10-μm thickness after 4 days of immersion, while only a few calcium phosphate particles were observed on annealing TiO_2 nanotubes immersed in the same solution for the same duration. Tensile testing showed that the bonding strength between HA coating and substrate was 27.2 ± 1.6 MPa. This treatment dramatically improved efficiency for promoting HA formation on anodic TiO_2 nanotubes at room temperature.

I. INTRODUCTION

TITANIUM and its alloys are widely applied in orthopaedic and orthodontic implants owing to their excellent mechanical properties, adequate corrosion resistance, and good biocompatibility.[1–4] Moreover, titanium and its alloys are bioinert materials, which can be covered by the host organism without being integrated with bone.[5,6] Thus, surface modification on titanium and its alloys was required and has been reported during the last several decades.[7–9] For example, chemical etching in either acidic or alkaline solutions or anodization above the breakdown potential to obtain a porous structure was reported by numerous groups.[10–15] Besides the etching and oxidation modification methods, different calcium phosphates (CaP), such as hydroxyapatite (HA, $Ca_{10}(PO_4)_6(OH)_2$), have been used often as a coating on titanium to improve its biocompatibility.[7,16–18] The plasma-sprayed HA-coated titanium alloys have been clinically applied.[19–21] However, reports describe the difficulty of controlling the quality, composition, and crystallinity of plasma-sprayed HA coatings.[22–24] An alternative dipping method was recently reported to form calcium phosphate coating by dipping and withdrawing the metallic implant in $Ca(OH)_2$ and $(NH_4)_2HPO_4$ solutions for various times, resulting in HA-covered surfaces. This method was applied to efficiently deposit synthetic HA after short-term immersion and can be applied on various porous metallic substrates such as aluminum and magnesium.[25]

Anodic oxidation is increasingly applied for surface treatment on titanium and its alloys to obtain nanotube structures at the surface. During the last decade, there have been numerous studies on the formation of TiO_2 nanotubes by anodization.[26–30] It was reported that the tubes with lengths ranging from 15 to 500 nm with about several micron thickness could be grown under anodic potentials ranging from 1 to 20 V in F^- containing acidic electrolyte,[26,27] resulting in TiO_2 nanotubes possessing a hollow structure for filling with bioactivating species and providing an interface suitable for anchoring connective tissue. It was reported that the TiO_2 nanotubes have many potential biomedical applications, for example, use as a bond scale and supporting platform for bone and stem cells, local delivery of antibiotics off-implant at the site of implantation, and the control of hemorrhaging by forming significantly stronger clots with reduced clotting times.[31–33]

Recently, HA coatings on TiO_2 nanotubes were developed for biomedical applications. It has been reported that HA coating was formed on the annealed TiO_2 nanotubes by immersion in 1.5 SBF (simulated biological fluid (SBF) with 1.5 times of Ca and P concentration than standard SBF) for 2 days. The resulting HA coating, however, was only about 10-nm thick.[30] Another study reported that HA could form on the titania nanotubes array when it was subjected to immersion in 5 M NaOH at 333 K (60 °C) for 24 hours

LU-NING WANG, PhD Candidate and JING-LI LUO, Professor, are with the Department Chemical and Materials Engineering, University of Alberta, Edmonton, AB, T6G 2V4 Canada. Contact e-mail: jingli.luo@ualberta.ca

or saturated $Ca(OH)_2$ for 6 hours followed by immersion in SBF.[34] However, there was a concern that the as-formed nanotube structure was dissolved or destroyed during the alkaline treatment, and it was difficult to identify the role of the damaged nanotube structure in the formation of HA.

It is believed that the nanostructure should be beneficial to tight adhesion of HA coating to titanium substrate and offer larger surface area for the nucleation of calcium and phosphate.[35] Therefore, a combination of the two methods, which are to apply the dipping method on the anodic TiO_2 nanotube layers and to form the HA coating, may form HA on TiO_2 nanotubes more efficiently than either method alone. In the present study, we investigated the possibility of filling the TiO_2 nanotubes with CaP nucleation sites using several dip-and-dry steps at room temperature, and investigated whether the treated tube layers showed an accelerated effect of HA formation when exposed to SBF. The coating was characterized and the mechanism of the formation is discussed.

II. EXPERIMENTAL PROCEDURES

A. *TiO_2 Nanotube Formation*

The sample material was Ti thin foil (99.6 pct purity, Alfa Aesar, Ward Hill, MA) with size of 1.0 cm × 1.0 cm and a thickness of 0.5 mm. Prior to anodization, the samples were ground with sandpaper up to 1200 grit and were ultrasonically rinsed with deionized (DI) water and ethanol for 20 minutes, sequentially, and then dried using compressed air at room temperature. The titanium specimen was rinsed in saturated H_2SO_4 for 1 minute to clean the surface before anodization. Anodization was conducted at room temperature in a two-electrode electrochemical cell with a graphite foil (1 cm × 1 cm) used as the counter electrode and 0.5 M H_3PO_4 + 0.5 wt pct NaF solution as the electrolyte. A direct current

Fig. 1—Schematic of the procedure for dipping treatment.

power supply (1715 A, B&K Precision Corporation, Yorba Linda, CA) was used as the voltage source to drive reactions involved in the anodization process. A constant 20 V potential was applied over a range of anodization periods. All as-prepared TiO_2 nanotube array films were rinsed using DI water and then dried using compressed air. In order to compare the materials formed using different treatments, some anodically treated samples were annealed at 723 and 823 K (450 and 550 °C) for 3 hours in air using a furnace with a heating rate of 10 K/min (10 °C/min).

B. *Dipping Method*

An accelerated calcium solution (ACS) was prepared by dissolving 8 g NaCl, 0.42 g $CaCl_2$, and 0.27 g $NaHPO_4$ in 1 L DI water.[36] The pH was adjusted to 7.4 by adding appropriate amounts of 1 M HCl and tris(hydroxymethyl)aminomethane (tris). The anodically treated specimen was vertically exposed in ACS for approximately 10 seconds and withdrawn from the solution with a wetting film remaining on the surface. The samples were placed on a slide glass and left to dry under flowing air for 10 minutes at room temperature. Every sample was treated up to 8 times followed by rinsing in DI water and drying in an air stream. The process of the dipping method is shown in Figure 1.

C. *HA Formation*

The HA formation of anodized TiO_2 nanotubes after dipping treatment was evaluated by immersion tests in a SBF (Table I).[37] The electrolyte with ionic concentrations similar to human plasma was prepared by dissolving reagent grade NaCl, KCl, $NaHCO_3$, $MgCl_2 \cdot 6H_2O$, Na_2SO_4, $CaCl_2$, and $K_2HPO_4 \cdot 3H_2O$ into DI water and buffered at pH = 7.25 with tris and HCl at 310 K (37 °C). The ratio of sample surface to the volume of SBF, S/V, was about 0.01 cm^{-1}. Separate samples were immersed in SBF for 12 hours, 2 days, and 4 days without stirring to investigate their bioactivity. After immersion, the samples were removed, rinsed with DI water, and dried in air.

D. *Surface Characterizations*

Field emission–scanning electron microscopy (FE-SEM) was used to determine surface morphology using a JEOL* JSM6301FXV SEM with a FE electron
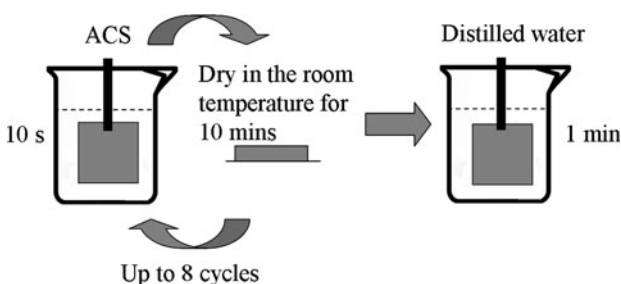
---

*JEOL is a trademark of Japan Electron Optics Ltd., Tokyo.

Table I. Ion Concentrations of SBF and Human Blood Plasma

	Concentrations (mM)							
	Na^+	K^+	Mg^{2+}	Ca^{2+}	Cl^-	HCO_3^-	HPO_4^{2-}	SO_4^{2-}
SBF	142.0	5.0	1.5	2.5	148.8	4.2	1.0	0.5
Blood plasma	142.0	5.0	1.5	2.5	103.0	27.0	1.0	0.5

source running at 5 kV and a JEOL field emission JAMP 9500F at 25 kV. X-ray photoelectron spectroscopy (AXIS Ultra XPS spectrometer, Kratos Analytical, Wharfside, Manchester, UK) was used to c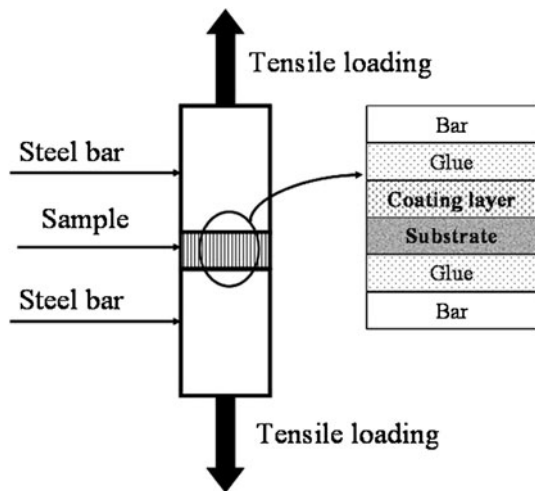haracterize the chemical composition of the surface. The XPS spectra were recorded using Al K_α radiation (1486.6 eV) as an excitation source. The composition and thickness of the TiO_2 nanotubes after dipping treatment were determined through time-of-flight–secondary ion mass spectrometry (ToF-SIMS) using an ION-ToF IV spectrometer. The compositions of the coating were determined with an energy dispersive X-ray (EDX) spectrometer and Fourier transform–infrared (FT-IR) spectrometer (Nicolet 8700, Thermo, Nepean, ON, Canada). The crystal structure was determined using a thin film–X-ray diffractometer (TF-XRD) with Cu K_α radiation. The bonding strength of the HA layer to the substrate was measured using a method described by Kim *et al.*, which is a modified ASTM C-633-08 method, through an Instron model 4505 universal testing system (Instron, Canton, MA).[38] Five samples were selected to obtain the bonding strength of the coating layer. Both sides of the sample were fixed to stainless steel square bars using rapid-type LePage glue, as shown in Figure 2. After the glue had fully dried, a continuous tensile load was applied vertical to the sample surfaces using a weight scale. The load (N) at which the coating separated from the substrate was recorded. The bonding strength was calculated by dividing the load at fracture by the sample surface area. The adhesive strength value (MPa) was taken as the average from five tested samples.
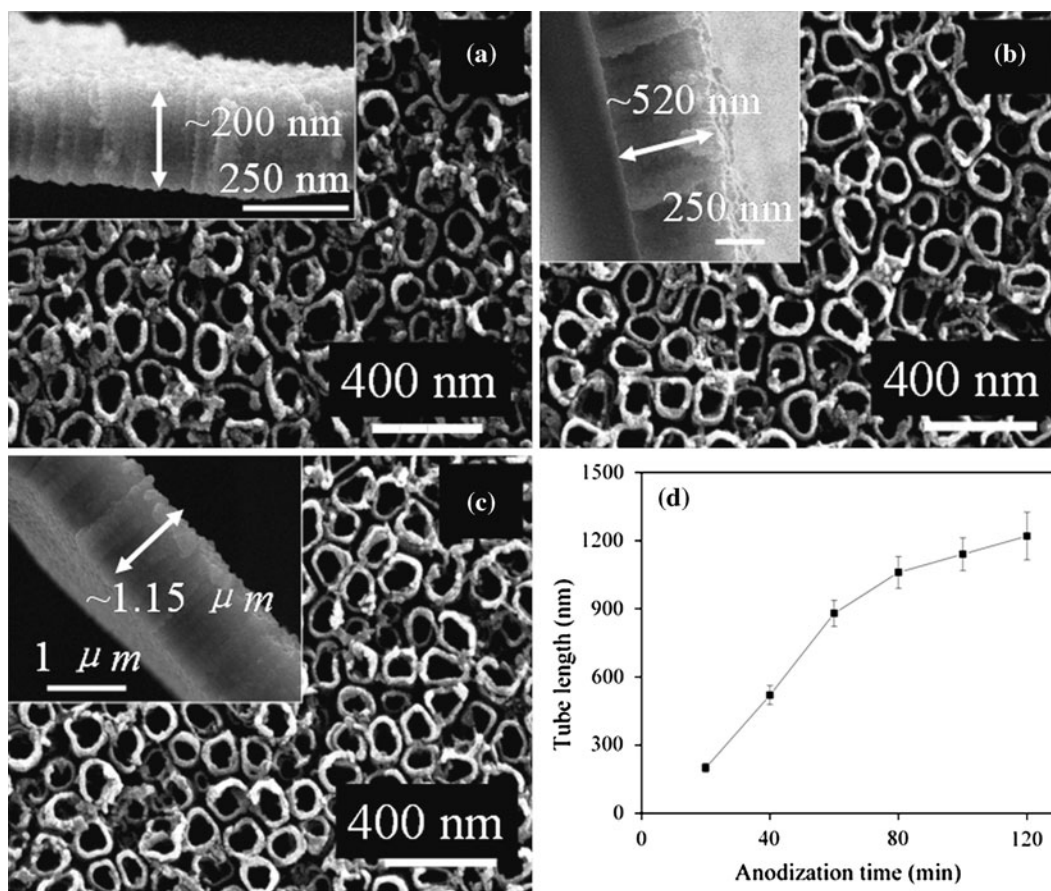

Fig. 2—Schematic of the bonding strength test of the HA coating to the substrate.

Fig. 3—FE-SEM images showing the top view and the side view (the inserts) of TiO_2 nanotubes after different anodization periods: (*a*) 20 min, (*b*) 40 min, and (*c*) 100 min. (*d*) The relationship between nanotube length and anodization period.

III. RESULTS

A. *Structure of TiO₂ Nanotubes*

Figure 3 shows examples of TiO₂ nanotubes formed at 20 V for different anodization periods, 20 minutes (Figure 3(a)), 40 minutes (Figure 3(b)), and 100 minutes (Figure 3(c)). The nanotubes have about 100-nm diameters and are distributed on the surface in a regular pattern. The inserted figures in Figures 3(a) through (c) portray side views of the cross sections of nanotubes. The tube layers were about 200 nm in thickness when the nanotubes were formed for 20 minutes, 520 nm after 40 minutes, and 1.15 μm after 100 minutes. The samples show that only the thickness, and not the diameter, of the tubes is a function of the anodization time. The thickness of the tubes as a function of anodization time is illustrated in Figure 3(d). The data show that the growth of TiO₂ nanotubes at 20 V increased rapidly in the initial stage, about 60 minutes. After the first 60 minutes, the growth of TiO₂ nanotubes gradually decreased and the nanotube length after anodization for 120 minutes was 1.22 μm. It is well accepted that the formation of TiO₂ nanotubes in F⁻ containing solution relies on three spontaneous processes: field-assisted oxidation of titanium to form titanium dioxide, field-assisted dissolution of titanium dioxide, and chemical dissolution of the TiO₂ by etching with fluoride ions.[29,32,33] It is believed that the final thickness of nanotube array is dominated by the dynamic equilibrium between the oxidation and the dissolution processes. As shown in Figure 3(d), the diffusion of fluoride anions through the short nanotubes to etch the titanium substrate to develop the TiO₂ nanotubes is relatively facile, as demonstrated in the first 60 minutes of anodization. However, as the tube lengthened, the diffusion of F⁻ in the tubes became increasingly difficult, with the consequence that longer time was required for ions to reach the bottom of TiO₂ and form the TiO₂ tubes. As a result, the rate of growth of the tubes decreased after 60 minutes, as shown in Figure 3(d). Since the tube length did not change much between the anodization periods from 100 and 120 minutes, the subsequent aspects of this work used anodized TiO₂ nanotube obtained at 20 V with 120 minutes.
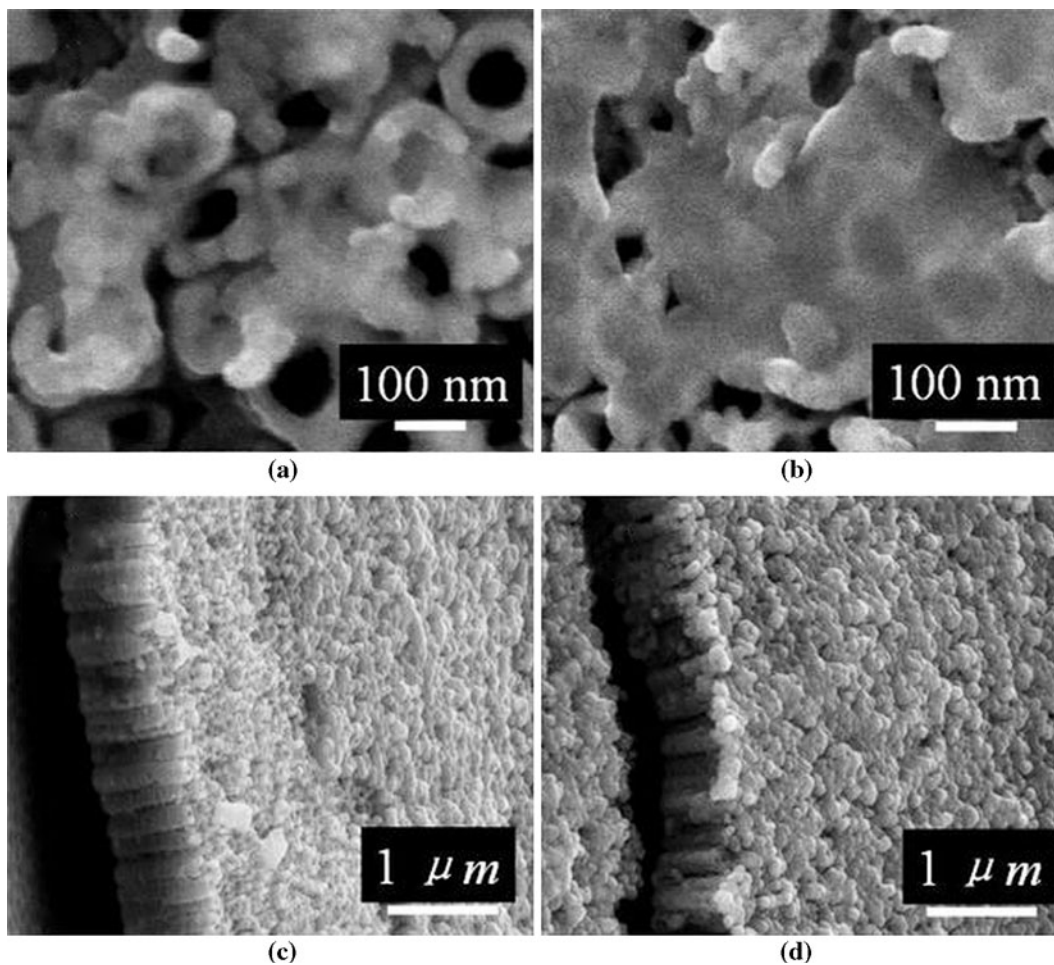

Fig. 4—FE-SEM images of TiO₂ nanotubes after different numbers of cycles of dipping treatment: (*a*) and (*c*) top view and side view, respectively, of the TiO₂ nanotubes after dipping twice; and (*b*) and (*d*) top view and side view, respectively, of the TiO₂ nanotubes after dipping eight times.

B. Dipping Effect on the Precipitation on TiO$_2$ Nanotubes

Figure 4 shows the top and side views of the nanotubes after dipping twice (Figure 4(a)) and 8 times (Figure 4(b)) in ACS solution. It clearly shows that some tubes are filled by deposition only after dipping twice. After 8 times of dipping, most of the tubes are filled and some tubes are even covered by the precipitations. As shown in the side view, one can clearly see the openings of tubes after dipping twice and fully covered surfaces after 8 times of dipping. XPS spectra further confirm the deposition of calcium and phosphate species (Figure 5(a)). The quantitative study of the amount of calcium is shown in Figure 5(b), and it suggests that 8 times of dipping treatment results in about 4 at. pct of calcium on the surface. Therefore, for the remaining portion of the study, the standard procedure was 8 times of dipping treatment. Figure 6 shows the ToF-SIMS depth profile of the specimen after 8 times of dipping treatment. Calcium and phosphate were enriched at the top surface and gradually decreased with depth, which indicated that calcium and phosphate penetrated well into the nanotubes.

C. Formation of HA Coating on TiO$_2$ Nanotubes with Dipping Treatment

Figure 7 shows SEM images of dipping-treated TiO$_2$ nanotubes after soaking in SBF for 12 hours, 2 days, and 4 days. It is clearly shown in Figure 7(a) that after 12 hours of immersion, the surface of the sample was already covered by a layer of flakelike particles. The inserted picture in Figure 7(a) shows a higher magnification image of the coating. Figure 7(b) shows the coating morphology after 2 days of immersion. It shows that the flakelike particles agglomerated to form a dense coating. Figure 7(c) and the inserted figure show the coating morphology and chemical compositions obtained after 4 days of immersion. Figure 7(c) shows typical spherical particles, which were similar to the HA formed in SBF, as described by others.[26,39,40] The EDX spectra demonstrated that the coating contained mainly Ca and P, and there was no peak for Ti, which indicated that the coating thickness was of the order of micrometers since there was no information from the substrate. Figure 7(d) shows a cross section of the coating layer. The coating was about 10 μm. For comparison purposes, separate samples of TiO$_2$ nanotubes were annealed for 723 K (450 °C) (Figure 8(a)) and 823 K (550 °C) (Figure 8(c)), and then immersed in SBF for 4 days. Their morphologies and the corresponding EDX spectra are shown in Figures 8(b) and (d). The nanotubes annealed at both temperatures were covered by very thin layers, and both EDX spectra showed mainly Ti peaks while the peaks for Ca and P were weak, which indicated that only a minor amount of calcium and phosphate was deposited on the surfaces. Figure 9 shows the TF-XRD results of the surfaces with different immersion periods in SBF. Figure 9(a) shows the spectrum of the intact substrate before immersion in SBF. The HA was detectable using TF-XRD after 2 days of immersion (Figure 9(b)). With prolongation of immersion time, the peaks of Ti gradually became weaker compared to those of HA, as shown in Figure 9(c), which indicated that calcium and phosphate were deposited onto the surface, formed HA crystals, and HA became thicker with immersion time. Figure 10
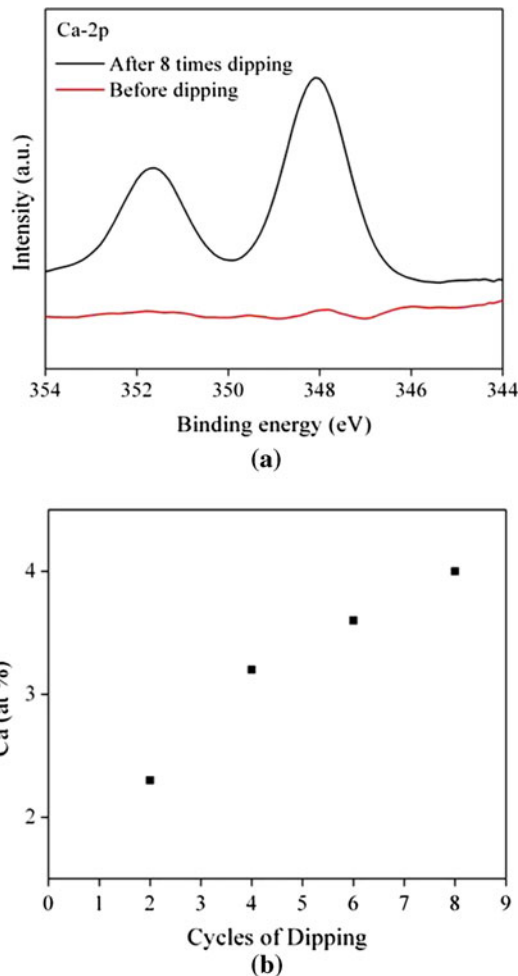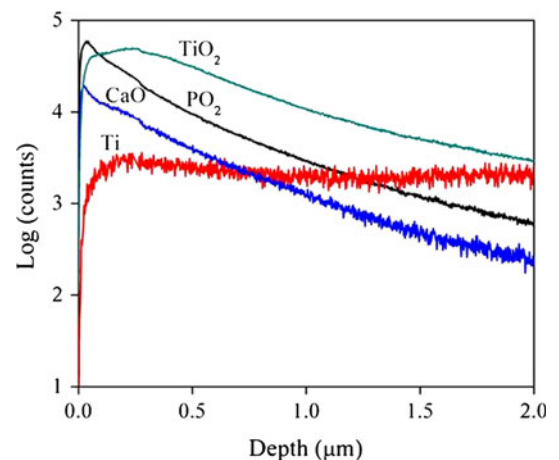
Fig. 5—(a) XPS spectra showing Ca-2p peaks before and after eight times dipping treatment. (b) Atomic concentration of Ca as a function of number of cycles of dipping treatment.

Fig. 6—SIMS spectra of the TiO$_2$ nanotube structure after eight times dipping.
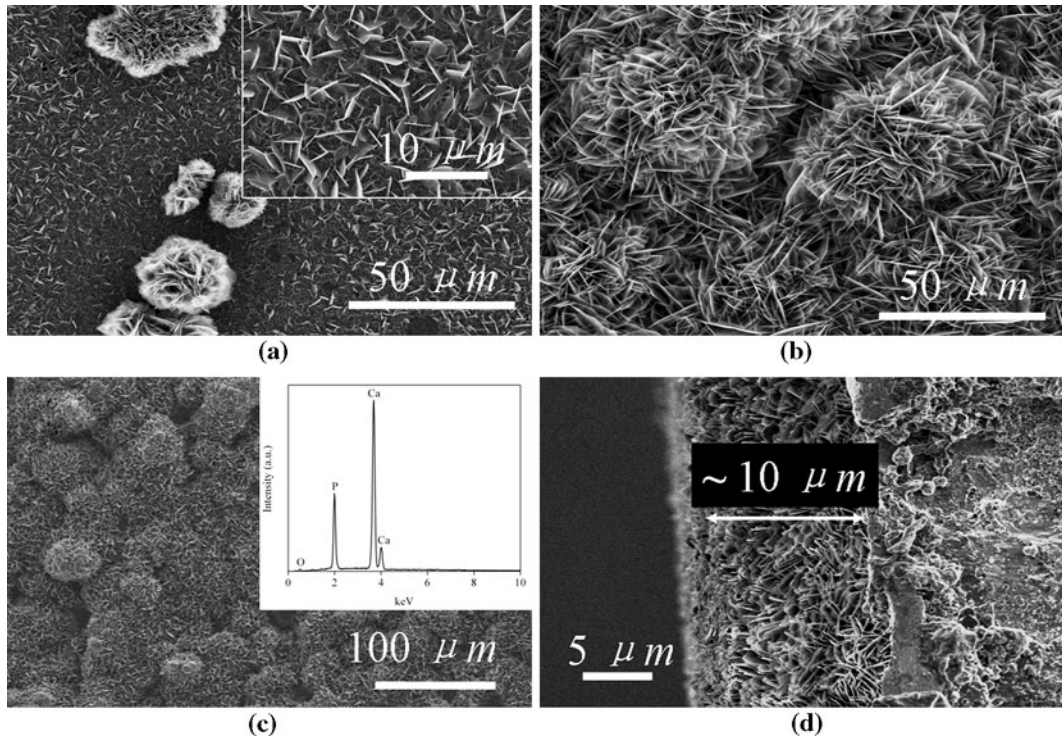
Fig. 7—SEM images of the TiO$_2$ nanotubes immersed in SBF for different periods: (*a*) 12 h, (*b*) 2 days, and (*c*) 4 days. (*d*) EDX spectrum corresponding to image (c).
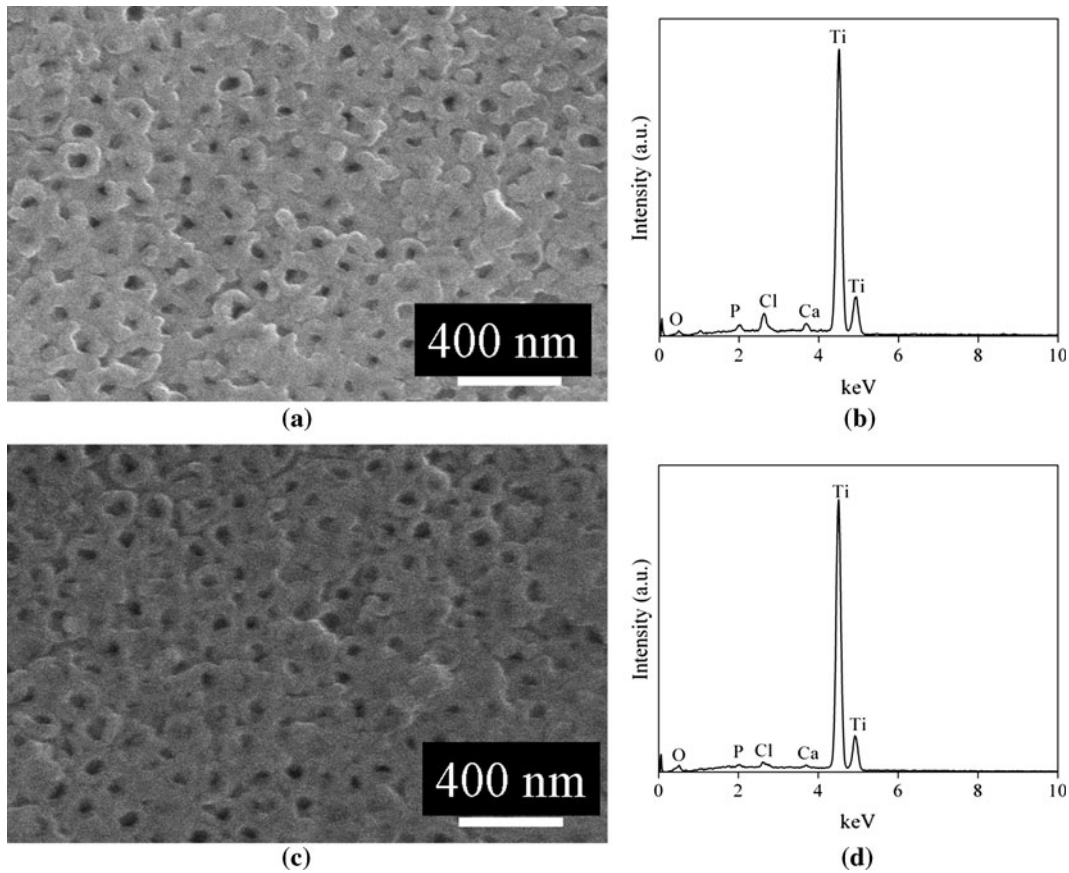

Fig. 8—SEM images of TiO$_2$ nanotubes (*a*) annealed at 723 K (450 °C) for 3 h and then immersed in SBF for 4 days and (*b*) the corresponding EDX spectrum; and (*c*) annealed at 823 K (550 °C) for 3 h and then immersed in SBF for 4 days and (*d*) the corresponding EDX spectrum.
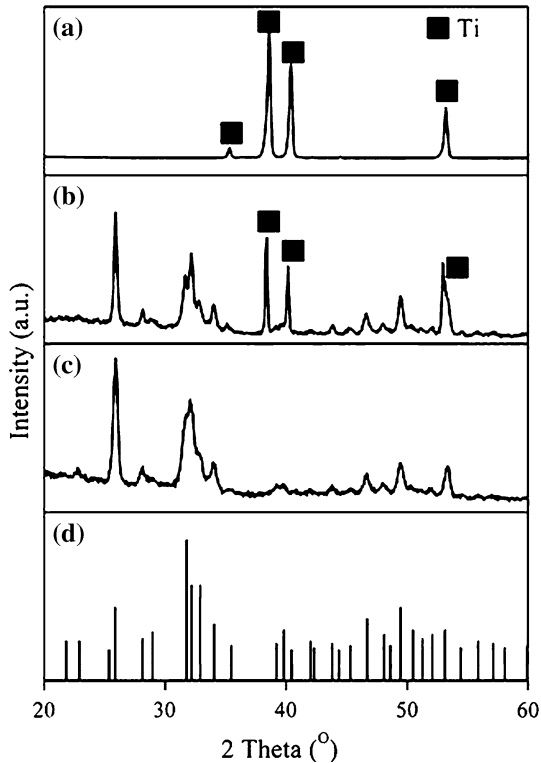
Fig. 9—TF-XRD patterns of the TiO₂ nanotube structure: (*a*) before treatment, (*b*) after immersion in SBF for 2 days, and (*c*) after 4 days, and the standard pattern for HA (JCPDF 09-0432).
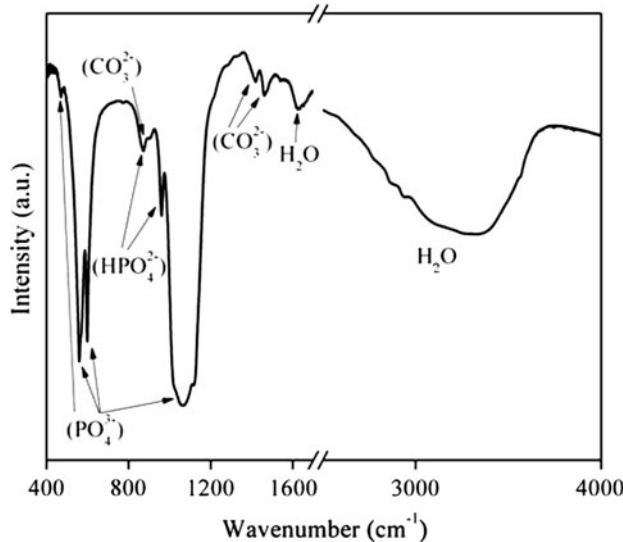

Fig. 10—FT-IR spectra of the HA coating on TiO₂ nanotubes with dipping treatment after 4 days of immersion in SBF.

shows the FT-IR spectrum of the HA coatings obtained after 4 days of immersion in SBF. The characteristic peaks of phosphate groups, molecular and adsorbed water bands, and hydroxyl groups became apparent in the spectrum, as summarized in Table II. Moreover, carbonate bands also were detected at 1420 and 1460 cm⁻¹. Therefore, the coating is carbonated HA.[41,42]

**Table II. Characterization of Materials from FT-IR Spectra**

Groups	Wave Number of Vibration Peak (cm⁻¹)
Bending mode of PO_4^{3-}	474, 567, and 604
Vibration of HPO_4^{2-}	875 and 958
Bending mode of CO_3^{2-}	875
Stretching mode of PO_4^{3-}	960 to 1200
Vibration of CO_3^{2-} on PO_4^{3-} lattice site	1420 and 1460
Bending mode of H_2O vibration	1645
Vibration of adsorbed H_2O	2500 to 3600

### D. *Bonding Strength of the HA Coating*

The bonding strength of the HA coating on TiO₂ nanotubes after 4 days of immersion in SBF was evaluated using the method described in Section II-D. The bonding strength of the HA coating on titanium dioxide nanotubes was 27.2 ± 1.6 MPa. The coating thickness was about 10 μm, a value consistent with that reported by Kim *et al.* for bonding strength of HA coating on alkaline-treated Ti substrate, about 27 MPa.[38] It was reported that bonding strengths of HA coatings on Bioglass and glass-ceramic A-W were less then 10 MPa.[38] Figure 11 compares bonding strengths of our result with others (Figure 11(a)), the SEM morphology (Figure 11(b)), and the EDX mapping of different elements, Ca, P, and Ti, on the fracture surfaces of substrates (Figures 11(c) through (e)). The bonding strength in this work, 27.2 MPa, is higher than the value, 15 MPa, of the ISO standard 13779-2:2008[43] for surgery apatite coating implants. From the EDX mapping, it can be seen that the intensities of reflected Ca and P peaks are strong on the fractured surface of the substrate, and Ti was hardly detected, which indicated that the HA adhered well to the substrate and the fracture happened within the HA coating layer but not along the interface between HA and TiO₂ nanotubes.

IV. DISCUSSION

In this study, the sequential dipping treatment induced deposition of calcium and phosphate before immersion in SBF and resulted in rapid HA formation on the titanium dioxide nanotubes structures. The mechanism of the dipping treatment tentatively proposed is an evaporation-induced process, shown in Figure 12, using a single tube as an example. The initial dipping step leaves a wetting film in the surface. Since the nanotube structure has a small diameter, a large pressure differential is generated across the liquid interface, so the ACS has a high surface tension similar to water and produces a large pressure difference described by the Young–Laplace equation.[35] Thus, the ACS can penetrate into the nanotubes due to the capillary effect. Consequently, the wetting film will in-fill
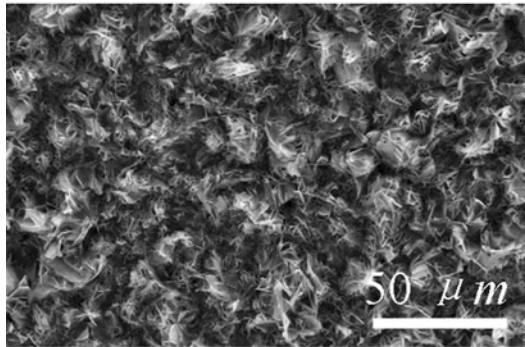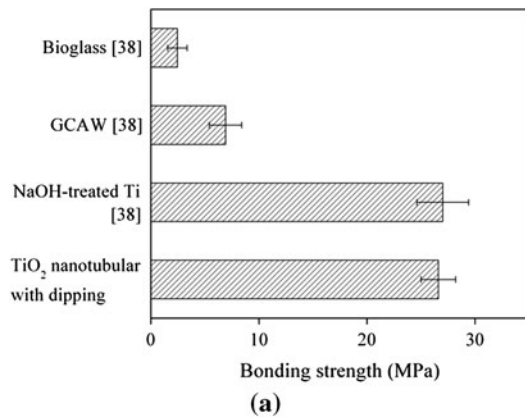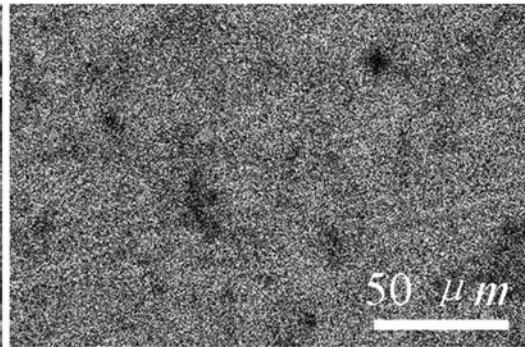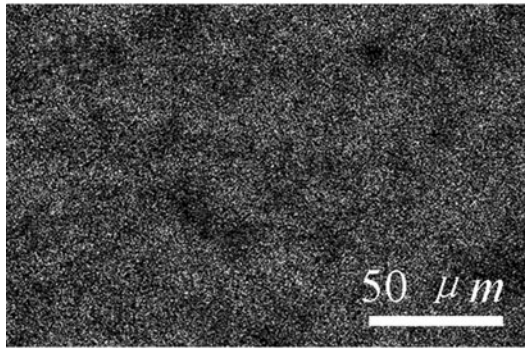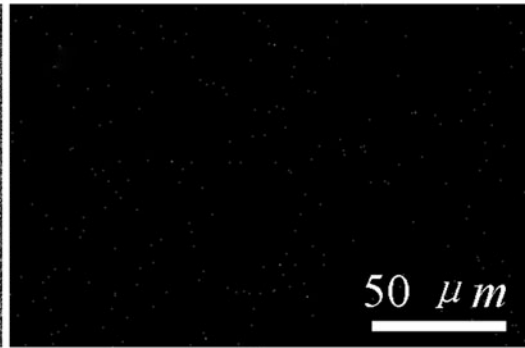
Fig. 11—(a) Comparison of the tensile bonding strengths of HA layers bonded to different substrates; (b) FE-SEM image of the fracture surface of the substrate; and EDX mapping of the elements (c) Ca, (d) P, and (e) Ti at the fracture surface.

and cover the inner wall of the nanotubes. During the drying step, the wetting film gradually evaporates resulting in an increasing supersaturation within the tubes. The supersaturation will induce calcium and phosphate depositions to form CaP crystallites adhering to the inner wall of the TiO_2 nanotubes (e.g., Figure 12(b)). The CaP may also react or interact with the other chemicals, such as NaCl, KCl, tris, etc. in the wetting film. These CaPs can be identified as those nonadhesive CaP particles within the tubes. The next dipping step makes the chemicals dissolve, nonadhesive CaP particles detach, and a new wetting film form. The repeated dipping treatment thus formed CaP-crystallite-covered inner walls of nanotubes, corresponding to the SIMS spectra shown as Figure 6. These CaP crystallites serve as nucleation sites for the generation of HA coating.

It was reported by Tsuchiya et al. that HA formed on the annealing TiO_2 nanotubes without pretreatment after 14 days of immersion in SBF.[26] The same group also reported that HA can form on TiO_2 nanotubes over 2 days by applying SBF10 after preloading HA treatment.[44] Feng et al. reported that an HA coating formed on annealing TiO_2 by immersion in SBF3 for 4 days.[35] From their results, either annealing of as-formed TiO_2 or a saturated SBF (SBF10 or SBF3) was required to obtain the HA coating within 4 days. In this study, a typical SBF was used and HA formed on substrate over 12 hours and had about 10-μm thickness within 4 days. The data herein indicate that TiO_2 nanotubes after the dipping treatment are fully covered by CaP nucleation sites. Therefore, the surface must have been supersaturated with calcium and phosphate once it was immersed in SBF, ready for the deposition of
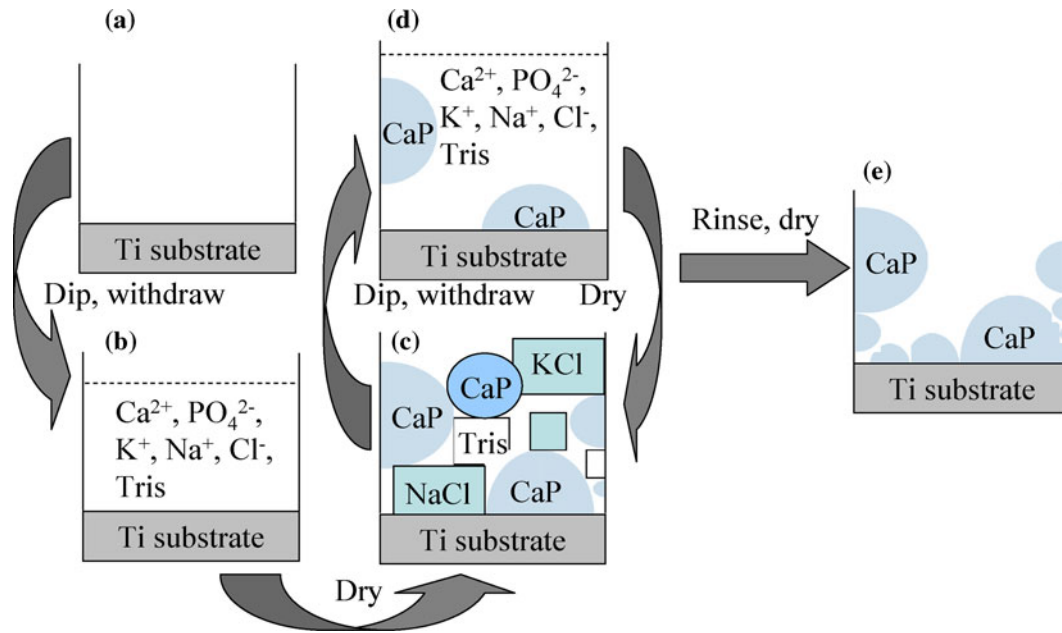
Fig. 12—Proposed mechanism of the dipping treatment on the TiO$_2$ nanotube: (*a*) the Ti substrate with the TiO$_2$ nanotubes dips and withdraws in the ACS; (*b*) a wetting film filled in the nanotube structure; (*c*) the film dries and results in the formation of CaP crystalline and other chemical crystalline, such as NaCl, KCl, and tris (some CaP adheres to the nanotubes); (*d*) during the repeated dip-and-withdraw procedures, more and more CaP forms and adheres to the nanotubes; and (*e*) the formation of CaP crystalline covers nanotubes after rinsing and drying (adapted from Refs. 25, 44 and 49).

calcium and phosphate, which then was converted rapidly to HA. The obtained HA coating was carbonated HA after 2 days of immersion. It has been suggested that carbonated HA was formed after immersion in CO$_3^{2-}$ containing SBF. The vibration bands at 1420 and 1460 cm^{-1} showed that (CO$_3^{2-}$) was partly substituted for (PO$_4^{3-}$), resulting in the formation of B-type carbonated HA, which is predominant in biological bone tissues.[45–47]

The mechanical properties such as tensile bonding strength of the calcium phosphate coating to substrate are important aspects of the coating properties.[12] As shown in Figure 11(a), the HA coating on TiO$_2$ nanotubes in this study had high bonding strength and was tightly bonded to the substrate, while remaining HA coating. EDX mapping (Figures 11(c) through (e)) also confirmed that the fracture of the coating happened within the HA coating, not between layers. The high bonding strength can be explained as follows. Since the TiO$_2$ nanotubes are filled with CaP nucleation sites after dipping treatment, the HA formed from the inside of the nanotubes. The structure of the coating then gradually changed from Ti substrate to TiO$_2$ nanotubes with HA coatings. The gradual change of the structure resulted in a high bonding strength. It has been reported that after the glass-ceramic A-W with CaP layer was implanted as a rabbit tibia for 1 month and a tensile stress was applied on the bone, the fracture occurred within the bone but not at the bone-implant surface.[48] This result demonstrated that even the glass-ceramic A-W with CaP layer contained enough bonding strength after implantation. The present work showed that HA coating formed on TiO$_2$ nanotubes had even higher bonding strength, which indicated that the HA coating with TiO$_2$ can bond very tightly to the living bone.

V. CONCLUSIONS

1. Titanium dioxide nanotubes structures were fabricated by anodization in F$^-$ containing electrolyte at 20 V. The anodization duration did not affect the nanotube diameter, only the length of the nanotubes. The tube length was increased in the initial stage of anodization and the rate of growth gradually decreased after about 1 hour of anodization.
2. A combination treatment with dipping method and anodized TiO$_2$ nanotubes developed in this work forms strongly bonded coatings. The HA coating readily formed on Ti implant materials with this treatment shortly after 12 hours of immersion in SBF. After 4 days of immersion in SBF, the HA typically formed spherical particles that fully covered the surface. The thickness of the HA coating was about 10 μm. FT-IR showed that the coating was carbonated HA.
3. The tensile bonding strength of the HA coating on Ti with TiO$_2$ nanotubes after 4 days of immersion in SBF was about 27.2 $\pm$ 1.6 MPa.
4. The combination of anodization to form TiO$_2$ nanotubes and the dipping method on Ti implant materials strongly accelerated HA formation on as-formed TiO$_2$ nanotubes when immersed in SBF. Therefore, the combined treatment was an efficient way to enhance the rate of HA formation on titanium biomaterials. Additionally, the results are

consistent with an evaporation based mechanism and resulted in CaP nucleation sites attached to the TiO$_2$ nanotubes.

REFERENCES

1. N. Sykaras, A.M. Iacopino, V.A. Marker, R.G. Triplett, and R.D. Woody: *J. Oral. Max. Impl.*, 2000, vol. 11, pp. 675–90.
2. A.C. Fraker: *Corrosion and Degradation of Implant Materials, 2nd Int. Symp.*, A.C. Fraker and C.D. Griffin, eds., ASTM, Philadelphia, PA, 1985, pp. 384–90.
3. S. Tamilselvi, V. Raman, and N. Rajendran: *Electrochim. Acta*, 2006, vol. 52, pp. 839–46.
4. W. Österle, D. Klaffke, M. Griepentrog, U. Gross, I. Kranz, and C. Knabe: *Wear*, 2008, vol. 264, pp. 505–17.
5. M. Textor, C. Sittig, V. Frauchiger, S. Tosatti, and D. Brunette: in *Titanium in Medicine: Materials Science, Surface Science, Engineering, Biological Responses and Medical Applications*, D. Brunette, D. Tengvall, M. Textor, and P. Thomsen, eds., Springer-Verlag, Berlin, 2001, pp. 171–244.
6. Y. Han, S.-H. Hong, and K. Xu: *Surf. Coat. Technol.*, 2003, vol. 168, pp. 249–58.
7. R. Wang and K. Duan: *J. Mater. Chem.*, 2006, vol. 16, pp. 2309–24.
8. X. Liu, P.K. Chu, and C. Ding: *Mater. Sci. Eng. R*, 2004, vol. 47, pp. 49–124.
9. Y. Yang, J.L. Ong, and J. Tian: *Biomaterials*, 2003, vol. 24, pp. 619–27.
10. X. Zhao, X. Liu, and C. Ding: *J. Biomed. Mater. Res.*, 2005, vol. 75A, pp. 888–94.
11. D.K. Pattanayak, T. Kawai, T. Matsushita, H. Takadama, T. Nakamura, and T. Kokubo: *J. Mater. Sci. Mater. Med.*, 2009, vol. 20, pp. 2401–11.
12. H.-M. Kim, F. Miyaji, T. Kokubo, and T. Nakamura: *J. Biomed. Mater. Res.*, 1996, vol. 32, pp. 409–17.
13. A. Rakngarm, Y. Miyashita, and Y. Mutoh: *J. Mater. Sci. Mater. Med.*, 2008, vol. 19, pp. 1953–61.
14. B. Yang, M. Uchida, H.-M. Kim, X. Zhang, and T. Kokubo: *Biomaterials*, 2004, vol. 25, pp. 1003–10.
15. A. Arvidsson, V. Franke-Stenport, M. Andersson, P. Kjellin, Y.-T. Sul, and A. Wennerberg: *J. Mater. Sci. Mater. Med.*, 2007, vol. 18, pp. 1945–54.
16. Q. Tang, R. Brooks, N. Rushton, and S. Best: *J. Mater. Sci. Mater. Med.,* DOI:10.1007/s10856-009-3841-y.
17. M.A. Lopez-Heredia, P. Weiss, and P. Layrolle: *J. Mater. Sci. Mater. Med.*, 2007, vol. 18, pp. 381–90.
18. P. Habibovic, F. Barrère, C.A. Van Blitterswijk, K. De Groot, and P. Layrolle: *J. Am. Ceram. Soc.*, 2002, vol. 85, pp. 517–22.
19. K. De Groot, R. Geesink, C.P. Klein, and P. Serekian: *J. Biomed. Mater. Res.*, 1987, vol. 21, pp. 1375–81.
20. Y.C. Tsui, C. Doyle, and T.W. Clyne: *Biomaterials*, 1998, vol. 19, pp. 2015–29.
21. Y.C. Tsui, C. Doyle, and T.W. Clyne: *Biomaterials*, 1998, vol. 19, pp. 2031–43.
22. K.A. Gross and C.C. Berndt: *J. Biomed. Mater. Res.*, 1998, vol. 39, pp. 580–87.
23. Y.C. Yang and E. Chang: *Biomaterials*, 2001, vol. 22, pp. 1827–36.
24. A. Tonino, C. Oosterbos, A. Rahmy, M. Therin, and C. Doyle: *J. Bone Jt. Surg. Am.*, 2001, vol. 83, pp. 817–25.
25. S. Ono, A. Kiyotake, and H. Asoh: *ECS Trans.*, 2008, vol. 11, pp. 1–8.
26. H. Tsuchiya, J.M. Macak, L. Müller, J. Kunze, F. Müller, P. Greil, S. Virtanen, and P. Schmuki: *J. Biomed. Mater. Res.*, 2006, vol. 77A, pp. 534–41.
27. S. Bauer, S. Kleber, and P. Schmuki: *Electrochem. Commun.*, 2006, vol. 8, pp. 1321–24.
28. A. Ghicov, H. Tsuchiya, J.M. Macak, and P. Schmuki: *Electrochem. Commun.*, 2005, vol. 7, pp. 505–08.
29. J. Tao, J. Zhao, C. Tang, Y. Kang, and Y. Li: *New J. Chem.*, 2008, vol. 32, pp. 2164–68.
30. J. Kunze, L. Müller, J.M. Macak, P. Greil, P. Schmuki, and F.A. Müller: *Electrochim. Acta*, 2008, vol. 53, pp. 6995–7003.
31. J. Park, S. Bauer, K.A. Schlegel, F.W. Neukam, K. Von Der Mark, and P. Schmuki: *Small*, 2009, vol. 5, pp. 666–71.
32. K. Das, A. Bandyopadhyay, and S. Bose: *J. Am. Ceram. Soc.*, 2008, vol. 91, pp. 2808–14.
33. J. Park, S. Bauer, K. Von Der Mark, and P. Schmuki: *Nano Lett.*, 2007, vol. 7, pp. 1686–91.
34. X. Xiao, T. Tian, R. Liu, and H. She: *Mater. Chem. Phys.*, 2007, vol. 106, pp. 27–32.
35. B. Feng, X. Chu, J. Chen, J. Wang, X. Lu, and J. Weng: *J. Porous Mater.*, DOI:10.1007/s10934-009-9307-2.
36. H.B. Wen, Q. Liu, J.R. De Wijn, K. De Groot, and F.Z. Cui: *J. Mater. Sci. Mater. Med.*, 1998, vol. 9, pp. 121–28.
37. T. Kokubo and H. Takadama: *Biomaterials*, 2006, vol. 27, pp. 2907–15.
38. H.-M. Kim, F. Miyaji, T. Kokubo, and T. Nakamura: *J. Biomed. Mater. Res. Appl. Biomater.*, 1997, vol. 38, pp. 121–27.
39. M. Uchida, H.-M. Kim, T. Kokubo, S. Fujibayashi, and T. Nakamura: *J. Biomed. Mater. Res.*, 2003, vol. 64A, pp. 164–70.
40. D.K. Pattanayak, T. Kawai, T. Matsushita, H. Takadama, T. Nakamura, and T. Kokubo: *J. Mater. Sci. Mater. Med.*, 2009, vol. 20, pp. 2401–11.
41. R. Horváthová, L. Müller, A. Helebrant, P. Greil, and F.A. Müller: *Mater. Sci. Eng. C*, 2008, vol. 28, pp. 1414–19.
42. C. Rey, C. Combes, C. Drouet, H. Sfihi, and A. Barroug: *Mater. Sci. Eng. C*, 2007, vol. 27, pp. 198–205.
43. "Implants for surgery-hydroxyapatite-part 2: Coating of hydroxyapatite," ISO 13779-2 2008, second edition.
44. A. Kodama, S. Bauer, A. Komatsu, H. Asoh, S. Ono, and P. Schmuki: *Acta Biomater.*, 2009, vol. 5, pp. 2322–30.
45. E. Landi, G. Celotti, G. Loggroscino, and A.J. Tampieri: *J. Euro. Ceram. Soc.*, 2003, vol. 23, pp. 2931–37.
46. I.R. Gibson and W. Bonfield: *J. Biomed. Mater. Res.*, 2002, vol. 59, pp. 697–708.
47. S.M. Barinov, J.V. Rau, S. Nunziante Cesaro, J. Ďurišin, I.V. Fadeeva, D. Ferro, L. Medvecky, and G. Trionfetti: *J. Mater. Sci. Mater. Med.*, 2006, vol. 17, pp. 597–604.
48. T. Nakamura, T. Yamamuro, S. Higashi, T. Kokubo, and S. Itoo: *J. Biomed. Mater. Res.*, 1985, vol. 19, pp. 685–98.
49. K. Duan, A. Tang, and R. Wang: *Mater. Sci. Eng. C*, 2009, vol. 29, pp. 1334–37.